

Torsional oscillations of crystalline color-superconducting hybrid stars: Possible sources for Advanced LIGO?

Lap-Ming Lin*

*Department of Physics and Institute of Theoretical Physics,
The Chinese University of Hong Kong, Hong Kong, China*

(Dated: October 18, 2018)

Deconfined quark matter may exist in a crystalline color-superconducting phase in the interiors of compact stars. In this paper, we study the torsional oscillations of compact stars featuring a crystalline color-superconducting quark-matter core in general relativity. Depending on the size of the crystalline core and the value of the gap parameter Δ , we find that the frequencies of the torsional oscillation modes can range from a few hundred hertz to a few kilohertz for our canonical $1.4M_{\odot}$ compact star models. We have also studied the prospect for detecting the gravitational-wave signals emitted from these modes in a pulsar glitch event. Assuming that at least 10% of the energy released in a Vela glitch can be channeled to the oscillation modes, we find that the Einstein Telescope should be able to detect these signals in quite general situations. Furthermore, if the size of the crystalline core is comparable to the stellar radius and the gap parameter is relatively small at $\Delta \sim 5$ MeV, the signal-to-noise ratio for Advanced LIGO could reach ~ 10 for a Vela glitch. Our optimistic results suggest that we might already be able to probe the nature of crystalline color-superconducting quark matter with the second-generation gravitational-wave detectors when they come online in the next few years.

PACS numbers: 04.30.Db, 25.75.Nq, 26.60.-c, 97.60.Jd

I. INTRODUCTION

With their densities reaching a few times the standard nuclear-matter density, the dense cores of compact stars have long been recognized as the most promising places where different exotic phases of matter could exist. In particular, in the early 1970s, it was speculated that the combinations of long-range attractive and short-range repulsive channels of neutron-neutron interactions might lead to a crystallization of nuclear matter (see Chap. 7 of [1] for a brief review). One of the applications of the possibility of solid cores inside neutron stars is the core-quake theory for pulsar glitches [2, 3]. It was also pointed out by Dyson already in 1972 that, if solid cores exist inside neutron stars, core quakes of these stars should excite torsional oscillations which might generate detectable gravitational-wave signals on Earth [4]. However, improved nuclear many-body calculations in the middle of 1970s essentially ruled out the possibility of crystallization of nuclear matter inside neutron stars.

Another exotic phase of matter inside compact stars proposed in the 1970s is the deconfined phase of quark matter (e.g., [6–8]). Thanks to our improved understanding of the QCD phase diagram nearly forty years later today, we now know that the deconfined quark matter inside compact stars may also be in a crystalline phase, and hence the possibility of solid cores inside compact stars has regained interest in recent years. It is now generally believed that the deconfined quarks inside mature (cold) compact stars could form Cooper pairs and give rise to

color superconductivity [9–12] (see [13, 14] for reviews). At sufficiently high density, pairing between quarks of different colors and flavors are allowed and the system is said to be in the color-flavor-locked (CFL) phase [11]. However, at intermediate densities relevant to compact stars, the more favored phase is the crystalline color-superconducting quark matter with broken spatial symmetries [15–19]. The presence of this crystalline phase of quark matter in the core of compact stars should produce astrophysical signatures that are very different from those of traditional neutron stars with a fluid core. Being able to identify these signatures from observational data would provide us a unique way to probe the nature of QCD in the high, but not asymptotically high, density regime. In this work, we shall focus on the gravitational-wave signatures of these objects.

It has long been known that the gravitational-wave signals emitted from compact stars carry important information about the internal structure of the stars (see, e.g., [20–24]), and thus their detection would give us viable information on dense matter. Regarding compact stars featuring a core of crystalline color-superconducting quark matter, the gravitational-wave emission due to nonaxisymmetric distortions of the solid core have been studied and analyzed with the (nondetection) results of the LIGO scientific runs S3/S4 [25, 26] and S5 [27]. A general conclusion obtained from these works is that the gravitational-wave signals are within the reach of LIGO if the solid core is maximally strained. In this paper, on the other hand, we shall study the gravitational-wave signals emitted from the torsional oscillations of the solid core. As we shall see below, depending on the gap parameter and the size of the core, the frequencies of these oscillation modes can range from a few hundred hertz to

*Electronic address: lmlin@phy.cuhk.edu.hk

a few kilohertz. This frequency range is quite different from those standard fluid modes of traditional neutron stars, such as the f and p modes, with typical frequencies at a few kilohertz [28]. Their relatively low frequencies also put the torsional oscillation modes within the best sensitivity region of ground-based gravitational-wave detectors such as LIGO, VIRGO, and KAGRA.

The plan of the paper is as follows. In Sec. II, we summarize the formulation that we employ to calculate the torsional oscillations of compact stars. Section III discusses the microphysical input that we need for constructing background stellar models and mode calculations. We present our numerical results in Sec. IV and discuss the prospect for detecting the gravitational-wave signals in Sec. V. Finally, we conclude our paper in Sec. VI. Unless otherwise noted, we use geometric units with $G = c = 1$.

II. FORMULATION

The formulation for studying torsional oscillations of compact stars in general relativity was first developed by Schumaker and Thorne [5] thirty years ago. A more recent gauge-invariant formulation of the problem can be found in [29]. Due to their relevance to the quasiperiodic oscillations in giant flares emitted from soft gamma-ray repeaters [30, 31], torsional oscillations in the solid crust of neutron stars have been studied in great detail recently (e.g., [32–38]). As far as we are aware, all these works are done within the Cowling approximation where the metric perturbations are neglected. This should be a good approximation in the study of oscillations in the crust of neutron stars, since the density is low in the crust and the spacetime variations should be small there. However, this is in general not necessarily true for the oscillations of a massive solid core. Hence, we shall employ the fully relativistic formulation of Schumaker and Thorne [5] to study the torsional oscillations, though we shall also compare the relativistic results with those obtained by the Cowling approximation.

In the following, we shall first summarize the standard set of equations for constructing the unperturbed equilibrium static configuration. We then briefly discuss the set of perturbation equations and numerical scheme for solving the torsional oscillation modes. We refer the reader to the original work [5] for the full derivations.

A. Equilibrium static background

The unperturbed background is assumed to be a static and spherically symmetric spacetime described by the metric

$$ds^2 = -e^{2\Phi(r)} dt^2 + e^{2\Lambda(r)} dr^2 + r^2(d\theta^2 + \sin^2\theta d\phi^2), \quad (1)$$

where the functions $\Phi(r)$ and $\Lambda(r)$ depend only on the radial coordinate r . The equilibrium structure of a compact star is determined by the standard Tolman-Oppenheimer-Volkov equations:

$$\frac{dm}{dr} = 4\pi r^2 \rho, \quad (2)$$

$$\frac{dP}{dr} = -\frac{(\rho + P)(m + 4\pi r^3 P)}{r^2(1 - 2m/r)}, \quad (3)$$

$$\frac{d\Phi}{dr} = \frac{m + 4\pi r^3 P}{r^2(1 - 2m/r)}, \quad (4)$$

where ρ and P are the energy density and pressure of the fluid, respectively. The function $m(r)$ is defined by $e^{-2\Lambda(r)} = 1 - 2m(r)/r$. With a given equation of state (EOS) $P(\rho)$, the above system of differential equations can be solved by imposing the boundary conditions (i) $m(0) = 0$; (ii) $P(R) = 0$; (iii) $e^{2\Phi(R)} = 1 - 2M/R$, where $M = m(R)$ is the total mass of the star and R is its radius.

B. Torsional perturbations

In studying the oscillation modes of compact stars, the metric and fluid perturbations are decomposed onto the basis of spherical harmonics [with indices (l, m)]. Without loss of generality, the study can be restricted to the $m = 0$ modes because the unperturbed background is spherically symmetric. Furthermore, the perturbations are in general distinguished into two classes according to their parities [39]: the so-called polar modes [with $(-1)^l$ parity] and axial modes [with $(-1)^{l+1}$ parity]. The torsional oscillation modes are of the latter class and hence we shall discuss the axial perturbations only. In the so-called Regge-Wheeler gauge, the axial metric perturbations $h_{\alpha\beta}$ can be expressed as

$$h_{\alpha\beta} = \begin{bmatrix} 0 & 0 & 0 & -r^2 \dot{y}(t, r) \\ 0 & 0 & 0 & -re^{\Lambda-\Phi} Q(t, r) \\ 0 & 0 & 0 & 0 \\ -r^2 \dot{y}(t, r) & -re^{\Lambda-\Phi} Q(t, r) & 0 & 0 \end{bmatrix} \sin\theta \frac{\partial}{\partial\theta} P_l(\cos\theta), \quad (5)$$

where $P_l(\cos\theta)$ is the Legendre polynomials of order l and the dot over $y(t, r)$ refers to derivative with respect

to t . The functions Λ and Φ are the background metric

functions defined in Eq. (1). On the other hand, the axial fluid perturbation is characterized by the displacement vector

$$\xi^r = 0, \quad \xi^\theta = 0, \quad \xi^\phi = \frac{Y(t, r)}{\sin\theta} \frac{\partial}{\partial\theta} P_l(\cos\theta). \quad (6)$$

To linear order in ξ^i , the four-velocity of the fluid is given by $u^\alpha = e^{-\Phi}(1, 0, 0, \xi^\phi)$.

The stress-energy tensor $T_{\alpha\beta}$ of the matter inside the star in general contains two contributions: $T_{\alpha\beta} = T_{\alpha\beta}^{\text{bulk}} + T_{\alpha\beta}^{\text{shear}}$. The bulk part $T_{\alpha\beta}^{\text{bulk}}$ is assumed to take the perfect fluid form

$$T_{\alpha\beta}^{\text{bulk}} = (\rho + P)u_\alpha u_\beta + P g_{\alpha\beta}. \quad (7)$$

The shear part $T_{\alpha\beta}^{\text{shear}}$ is given by

$$T_{\alpha\beta}^{\text{shear}} = -2\mu S_{\alpha\beta}, \quad (8)$$

where μ is the shear modulus and $S_{\alpha\beta}$ is the shear tensor which describes the deformations generated by the displacement ξ^i . The explicit expressions for $S_{\alpha\beta}$ can be found in [5]. In this work, we will consider star models in which there exists two regions: a crystalline quark-matter core and a nuclear-matter fluid envelope. The shear modulus μ , and hence $T_{\alpha\beta}^{\text{shear}}$, is nonzero only in the crystalline core. It should also be noted that ρ and P cannot support axial perturbations because they are scalar fields. Thus, our compact star models can support torsional oscillations only in their crystalline cores. Of course, a more realistic compact star model may also have a thin crust near the surface to support torsional oscillations. Since our focus is on the emitted gravitational-wave signals associated with torsional oscillations, which are dominated by the massive crystalline core, we shall thus neglect the crust in our study.

Assuming a time dependence $e^{i\omega t}$ for the fluid and metric perturbations [e.g., $Y(t, r) = Y(r)e^{i\omega t}$], the linearized fluid and Einstein field equations reduce to the following differential equations:

$$\begin{aligned} X' &= r^4 e^{\Phi+\Lambda} \left[16\pi(\rho + P) + \frac{(l+2)(l-1)}{r^2} \right. \\ &\quad \left. - \frac{\rho + P}{\mu} \omega^2 e^{-2\Phi} \right] \mu Y + (\mu - \rho - P) r^3 e^{\Lambda-\Phi} Z \\ &\quad + [r\mu' + 3\mu - (\rho + P)] r^2 Q, \end{aligned} \quad (9)$$

$$\begin{aligned} Z' &= 16\pi r (\mu e^{2\Phi})' Y + e^{\Phi+\Lambda} \left[16\pi\mu + \frac{l(l+1)}{r^2} \right. \\ &\quad \left. + 4\pi(\rho - P) - \frac{6m}{r^3} - \omega^2 e^{-2\Phi} \right] Q, \end{aligned} \quad (10)$$

where primes denote derivatives with respect to r . The auxiliary functions X and Z are defined by

$$X = \mu r^4 e^{\Phi-\Lambda} Y', \quad (11)$$

$$Z = e^{\Phi-\Lambda} Q'. \quad (12)$$

The above first-order system of equations are equivalent to Eqs. (50a) and (50b) in [5], though being expressed in terms of different variables. After solving the above equations for the mode frequency ω with appropriate boundary conditions (see below), the remaining metric perturbation function y can then be obtained by

$$y = \frac{1}{\omega^2} \left[\frac{-e^{\Phi-\Lambda}}{r^2} (rQ)' + 16\pi\mu e^{2\Phi} Y \right]. \quad (13)$$

The fact that y is decoupled from the wave equations (9) and (10), and being determined separately by Eq. (13), is traceable to the gauge choice used in the formulation as discussed in [29]. As we are only interested in obtaining the mode frequency ω , we shall not discuss the function y any further.

In the nuclear-matter fluid region outside the core, the shear modulus vanishes and the fluid cannot support torsional oscillations. In this region, the fluid only differentially rotates and the gravitational perturbation Q is completely decoupled from the fluid [39]. It can be shown that the governing equation for Q [Eq. (10)] in this region can be written as (with $\mu = 0$)

$$\frac{d^2 Q}{dr_*^2} = \frac{e^{2\Phi}}{r^3} [l(l+1)r + 4\pi r^3(\rho - P) - 6m] Q - \omega^2 Q, \quad (14)$$

where the Regge-Wheeler radial coordinate r_* is defined by $\partial/\partial r_* = e^{\Phi-\Lambda} \partial/\partial r$. This is the standard wave equation governing the so-called axial w modes of neutron stars, which are due to spacetime oscillations (see, e.g., [28] for a review). Outside the star where ρ and P vanish, Eq. (14) reduces to the Regge-Wheeler equation governing the perturbations of Schwarzschild spacetime:

$$\frac{d^2 Q}{dr_*^2} = \left(1 - \frac{2M}{r} \right) \left[\frac{l(l+1)}{r^2} - \frac{6M}{r^3} \right] Q - \omega^2 Q, \quad (15)$$

where $r_* = r + 2M \ln(r/2M - 1)$ and $M = m(R)$ is the mass of the star.

C. Boundary conditions and numerical methods

In order to calculate the torsional oscillation modes, the perturbation equations as listed in Sec. II B must be solved with suitable boundary conditions at the center, the solid-fluid interface, the stellar surface and at infinity. First, the regularity conditions of the fields at the center require that

$$Y \sim r^{l-1}, \quad Q \sim r^{l+1}, \quad (16)$$

near $r = 0$. At the solid-fluid interface $r = R_c$, we impose the zero-traction condition which is given by [5]

$$\mu (Y' - e^{\Lambda-\Phi} Q/r) = 0. \quad (17)$$

On the other hand, the continuity conditions of the intrinsic and extrinsic curvatures require Q to be continuous there and also at the stellar surface $r = R$. Outside the star, the Regge-Wheeler equation (15) has the asymptotic solution

$$Q \sim A_{\text{in}} e^{i\omega r_*} + A_{\text{out}} e^{-i\omega r_*}, \quad (18)$$

as $r_* \rightarrow \infty$. The quasinormal mode frequency ω is determined by requiring that there is only outgoing gravitational radiation at infinity (i.e., $A_{\text{in}} = 0$). Note that ω is in general a complex number because of the damping due to the emission of gravitational waves.

In the following, we outline our numerical scheme to obtain the mode frequency. Given an equilibrium background configuration and a trial frequency ω , we integrate Eqs. (9)-(12) in the solid core using initial conditions $Y(r) = Y_0 r^{l-1}$ and $Q(r) = Q_0 r^{l+1}$, where the ratio Y_0/Q_0 is set to some value. The integration is carried out to the solid-fluid interface $r = R_c$ at which we check whether the boundary condition there [Eq. (17)] is satisfied. If Eq. (17) is not satisfied, a new value of Y_0/Q_0 is used and the integration is repeated. Once a correct value of Y_0/Q_0 is found, we then integrate Eq. (14) in the fluid envelope and finally Eq. (15) in the vacuum. The trial frequency ω is the desired quasinormal mode solution if the asymptotic ingoing-wave amplitude A_{in} vanishes. In practice, we determine A_{in} from Eq. (18) at $r = 100R$ and the real parts of the mode frequencies are determined by the locations of deep minima in a graph of $\log_{10} |A_{\text{in}}|$ vs $\text{Re}(\omega)$.

As a demonstration of the graphical method, we show a typical result in our calculations in Fig. 1. The location of the minimum in the figure corresponds to the frequency of a torsional oscillation mode of the stellar model A (discussed in Sec. IV) with the gap parameter $\Delta = 10$ MeV. We refer the reader to [40–42] for similar applications of this graphical method. Since the torsional oscillation modes emit current-quadrupole gravitational waves, these modes are damped much more slower than polar fluid modes such as the f and p modes (as they emit mass-quadrupole waves). Hence, we need to use a high resolution along the ω axis in order to locate the modes. We typically set $\Delta\omega M < 10^{-7}$ in the calculations, where $\Delta\omega$ is the step size along the ω axis.

III. MICROPHYSICS INPUT

A. Equation of state

In order to construct equilibrium hybrid stars, we need to provide EOS models to describe the quark-matter core and nuclear-matter envelope. The quark-matter EOS is in general derived using the MIT bag model and its variations or more realistic Nambu-Jona-Lasinio (NJL) type models [43]. In our numerical calculations we use the simple phenomenological quark-matter EOS model of Alford

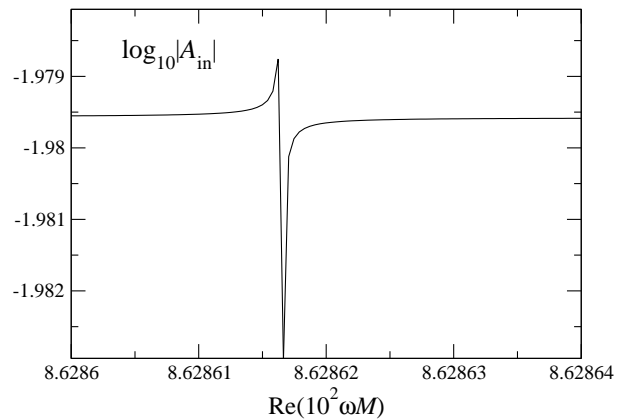


FIG. 1: Plot of A_{in} against $\text{Re}(\omega M)$ for a typical oscillation-mode calculation in this work. The location of the minimum gives the frequency of a mode.

et al. [44] for the quark core. The model is based on the thermodynamic potential

$$\Omega_{\text{QM}} = -\frac{3}{4\pi^2} a_4 \mu_q^4 + \frac{3}{4\pi^2} a_2 \mu_q^2 + B_{\text{eff}}, \quad (19)$$

where μ_q is the quark chemical potential. The phenomenological parameters a_4 , a_2 , and B_{eff} are independent of μ_q . The parameter $a_4 (\leq 1)$ is used to account for nonperturbative QCD corrections. The limiting case $a_4 = 1$ corresponds to three flavors of noninteracting quarks. The reasonable value for a_4 is expected to be of order 0.7 [44]. The parameter a_2 is used to model the effects of quark masses and pairing. Finally, the effective bag constant B_{eff} can be regarded as a parameter to control the density at which the transition from nuclear matter to quark matter occurs.

In the nuclear-matter envelope we use the model of Akmal *et al.* (APR) [45] at high densities. At lower densities, the APR EOS is matched to the model of Douchin and Haensel [46], which is followed by the model of Baym *et al.* [47] and Haensel and Pichon [48]. We implement the phase transition from nuclear matter to deconfined quark matter using a Maxwell construction. The EOS for the two different phases are matched by requiring that the pressures of both phases are equal at certain (baryonic) chemical potential.

We could in principle employ more sophisticated models for the quark core, such as the NJL model used in [27, 49] where the three-flavor crystalline phase of QCD is built in consistently. At this point we are more concerned with the technical developments of the numerical program and the qualitative properties of the torsional oscillation modes, so we focus only on the phenomenological model [Eq. (19)] as an illustrative example in this work.

Model	$a_2^{1/2}$ (MeV)	a_4	$B_{\text{eff}}^{1/4}$ (MeV)	ρ_c ($10^{15} \text{ g cm}^{-3}$)	R_c (km)	R (km)
A	100	0.85	160	1.487	8.28	10.31
B	100	0.8	160	1.265	4.71	11.07
C	200	0.9	150	1.205	1.71	11.24

TABLE I: The canonical background stellar models for the oscillation-mode calculations as discussed in the text. All models have the same total mass $1.4M_\odot$.

B. Shear modulus

The shear modulus of crystalline color-superconducting quark matter has been calculated by Mannarelli *et al.* [50] and is given by

$$\mu = 2.47 \text{ MeV/fm}^3 \left(\frac{\Delta}{10 \text{ MeV}} \right)^2 \left(\frac{\mu_q}{400 \text{ MeV}} \right)^2, \quad (20)$$

where Δ is the gap parameter. It should be pointed out that the result is obtained by performing a Ginzburg-Landau expansion to order Δ^2 . Since the control parameter for the expansion is about $1/2$ [50], Eq. (20) can thus be regarded as an estimation of μ only. For quark matter inside compact stars, the quark chemical potential μ_q is expected to lie in the range $350 \text{ MeV} < \mu_q < 500 \text{ MeV}$ [50, 51]. The gap parameter Δ is less certain and is expected to lie between 10 and 100 MeV in the CFL phase where the strange quark mass can be neglected. However, Mannarelli *et al.* [50] estimate that Δ should be in the range $5 \text{ MeV} \lesssim \Delta \lesssim 25 \text{ MeV}$ in order for the quark matter to be in the crystalline phase rather than the CFL phase. As a result, the shear modulus of crystalline color-superconducting quark matter is in the range $0.47 \text{ MeV/fm}^3 < \mu < 24 \text{ MeV/fm}^3$, which is much larger than that of the neutron star's crust [$\sim O(1 \text{ keV/fm}^3)$]. This is the reason why the maximum equatorial ellipticity sustainable by stellar models with a crystalline color-superconducting quark-matter core can be a few orders of magnitude larger than which can be supported by the neutron star's solid crust [25–27] (see also [52, 53] for relevant studies).

IV. NUMERICAL RESULTS

A. Equilibrium stellar models

In the oscillation-mode calculations, we need to first construct equilibrium stellar models which depend on the background EOS model. While the EOS for the nuclear fluid envelope is fixed in our calculations, there are still three free parameters (a_2 , a_4 , B_{eff}) in the quark-matter EOS for the core. Since the parameter space is vast and we are mainly interested in understanding the qualitative properties, we shall only use three different sets of parameters to construct three “canonical” background stellar

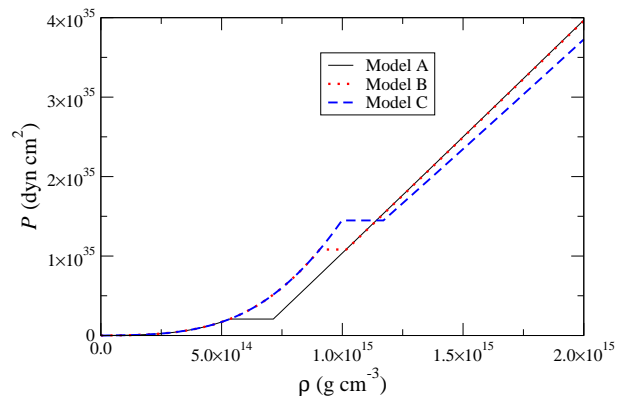


FIG. 2: Pressure is plotted against energy density for our EOS models.

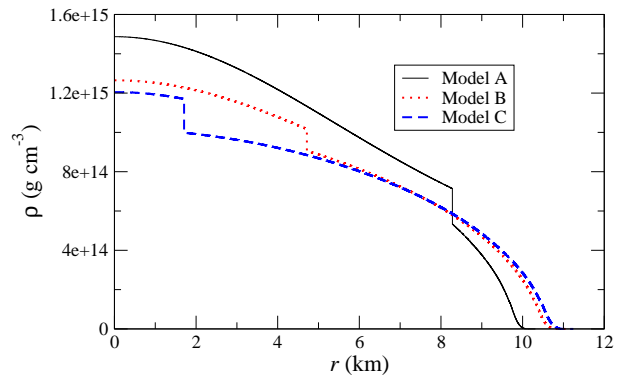


FIG. 3: Plot of the density profiles for the three background stellar models listed in Table I.

models with the same total mass $M = 1.4M_\odot$. The EOS parameters (a_2 , a_4 , B_{eff}), central density ρ_c , quark-core radius R_c , and stellar radius R of the background models are summarized in Table I.

The EOS parameters are chosen in order to produce quark-matter EOS models which can match to our fixed nuclear-matter EOS at low density as discussed in Sec. III A. Furthermore, the three sets of parameters are also chosen to yield significant differences in the internal structures of the stellar models for comparison. The effects of different parameters on the EOS can be seen in Fig. 2. In the figure, we plot the pressure against energy density for the three EOS models. It is note that, according to the Maxwell construction of the phase transition, there is in general a discontinuity in the energy density at constant pressure as shown in Fig. 2 (see also [44]). Figure 2 shows that the density at which the transition from nuclear matter to quark matter occurs, and also the jump in the density at the transition, depend quite sensitively on the EOS parameters. This leads to significant differences in the internal structures of the three background stellar models. In particular, by comparing models A and B, it can be seen that a small change in the value of a_4 can lead to a large difference in the density at which the phase transition occurs. In Fig. 3 we plot the density pro-

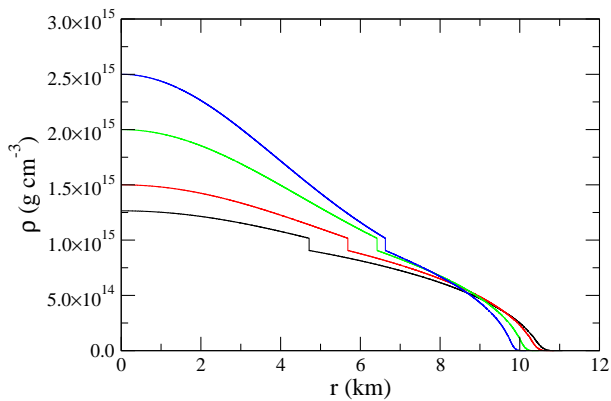


FIG. 4: Density profiles for stellar models with different central densities. The stars are constructed with the same EOS model B. The star with the lowest central density corresponds to our canonical model B listed in Table I. The star with the highest central density has a mass $1.63M_{\odot}$.

files of the three background models for comparison. In our oscillation-mode calculations, we shall consider how the size of the quark core for a $1.4M_{\odot}$ canonical stellar model affects the mode frequency. Model A thus represents the situation of a large quark core ($R_c/R \sim 0.8$), while model C represents the more conservative case of a small core ($R_c/R \sim 0.1$).

While we shall only focus on the three $1.4M_{\odot}$ stellar models in the oscillation-mode calculations, it is also interesting to see how the stellar structure would change for more massive configurations. In Fig. 4, we plot the density profiles for stellar models with different central densities. The stars are constructed with the same EOS model B. The profile with the largest central density in the figure corresponds to a $1.63M_{\odot}$ hybrid star. We note that for larger central densities, and hence more massive stars, the radius of the quark core becomes less sensitive to the central density and saturates at $R_c \sim 6.6$ km. We refer the reader to [27] for a similar trend observed in a NJL model where R_c saturates at 7 km for massive stars near $2M_{\odot}$.

Although our quark-matter EOS is based only on a phenomenological model, we believe that the resulting three stellar models are quite generic in representing the internal structures of crystalline color-superconducting hybrid stars. Our models are also compatible to the results obtained by the NJL model of [27, 49] in which it is shown that large crystalline quark cores ($R_c/R > 0.5$) can exist in compact stars.

B. Torsional oscillation modes

In this subsection we consider the $l = 2$ torsional oscillation modes of the three canonical stellar models presented in Sec. IV A. Our focus will be on how the size of the quark core and the gap parameter Δ affect the frequencies of the modes. In particular, we only consider

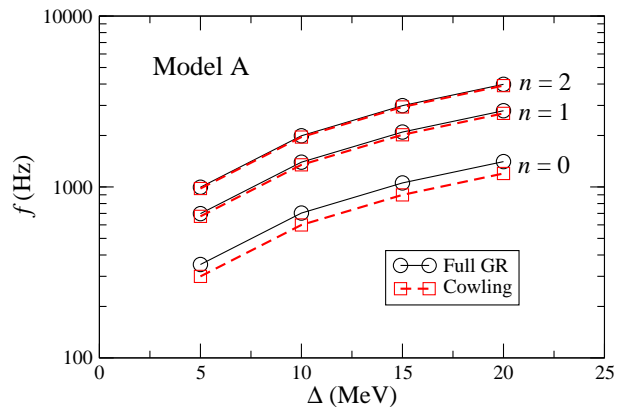


FIG. 5: Frequency of the torsional oscillation modes as a function of the gap parameter for the stellar model A listed in Table I. The integer n is the mode order (i.e., $n = 0$ corresponds to the fundamental mode and so on). The solid lines are computed using the fully relativistic framework as discussed in the text, while the dashed lines are obtained by neglecting the metric perturbations (Cowling approximation).

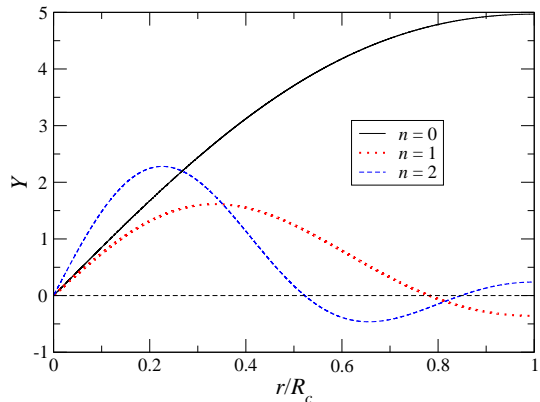


FIG. 6: Radial amplitudes of the fluid perturbation function Y inside the quark core for the torsional oscillation modes of stellar model A and $\Delta = 10$ MeV. The horizontal dashed line is used to pinpoint where the amplitudes vanish.

the range $5 \text{ MeV} \lesssim \Delta \lesssim 25 \text{ MeV}$ in our calculations as this is the theoretically allowed range as discussed in Sec. III B.

We begin by plotting in Fig. 5 the frequencies of the first three torsional oscillation modes of stellar model A against Δ . In the figure, the fundamental modes are given by the curves labeled as $n = 0$. Similarly, the first and second harmonics are given by the curves labeled as $n = 1$ and $n = 2$, respectively. The general pattern of the mode eigenfunctions can be seen in Fig. 6 in which we plot the fluid perturbation function Y inside the quark core for the case $\Delta = 10$ MeV. Note that the value of n corresponds to the number of nodes in the mode eigenfunctions.

In Fig. 5, the solid lines are the results obtained from the fully general relativistic calculations as discussed in Sec. II B. On the other hand, the dashed lines are ob-

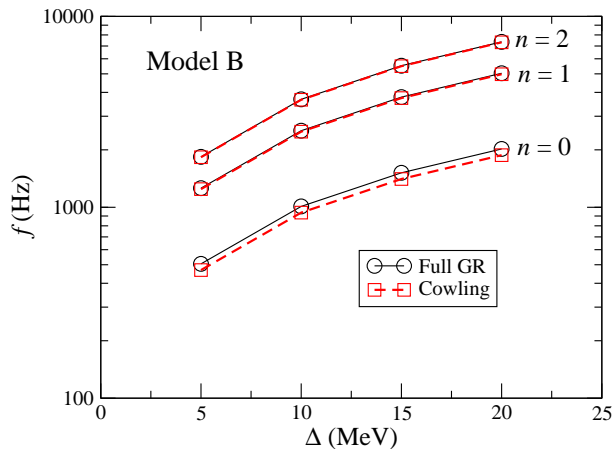


FIG. 7: Similar to Fig. 5, but for the stellar model B listed in Table I.

tained by using the Cowling approximation where the metric perturbations are neglected (see, e.g., [32, 37] for the relevant equations in the Cowling approximation). The relative differences between the fully relativistic and Cowling results are about 15% for the $n = 0$ fundamental modes. The differences are even smaller for the higher harmonics. We also note that the relative differences decrease as the size of the quark core shrinks. For instance, the fully relativistic and Cowling results for the fundamental modes of stellar model C, which has the smallest quark core among the three models, agree to about 1%.

Figure 5 also shows that the mode frequency f depends sensitively on Δ . In particular, the frequency of the fundamental mode ($n = 0$) increases from 351.8 to 1407.3 Hz as Δ increases from 5 to 20 MeV. Figure 7 plots the results of stellar model B for comparison. In particular, for a given stellar background model, our numerical results show that the mode frequency is proportional to Δ . This can be understood by noting that the frequency of a shear mode is given roughly by $f \sim v_s/2\pi R_c$, where the speed of the shear wave is $v_s = [\mu/(\rho + P)]^{1/2}$ [32]. Since the shear modulus μ is proportional to Δ^2 , the mode frequency is thus proportional to Δ as we found numerically.

The dependence of the mode frequency on the size of the quark core (and hence the quark-matter EOS parameters) can be seen in Fig. 8. In the figure, the fundamental modes for the three stellar models are plotted against Δ . As discussed above, models A and C have the largest and smallest quark core among the three models, respectively. It is thus expected that model A (model C) should have the lowest (highest) mode frequency for a given value of Δ as shown in Fig. 8, since the speeds of the shear waves for the three models do not differ significantly.

It is also interesting to notice that the fundamental-mode frequencies for models A and B are in the range from about a few hundred hertz to two kilohertz. This frequency range is quite different from those of the polar

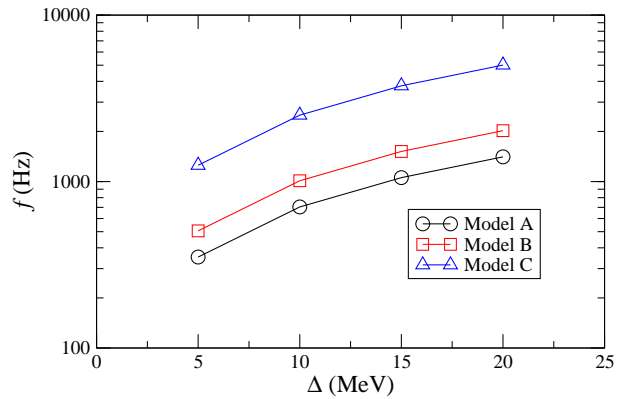


FIG. 8: This figure compares the fundamental ($n = 0$) mode frequencies of the three stellar models listed in Table I.

oscillation modes of traditional neutron stars, such as the f and p modes, which have higher frequencies at a few kilohertz or above. Hence, these torsional oscillation modes should be easily distinguished from those polar oscillation modes. Their relatively low frequencies also mean that these modes might already be detectable by the second-generation detectors such as Advanced LIGO, since the best sensitivities for these detectors are in the range of a few hundred hertz. We shall turn to this issue in the next section.

V. GRAVITATIONAL-WAVE DETECTION

The power carried by any weak gravitational wave of strain h is given by (see, e.g., [54])

$$\dot{E} = \frac{c^3 d^2}{4G} \dot{h}^2, \quad (21)$$

where the dots refer to time derivatives and d is the distance between the source and detector. Note that we have restored the constants G and c . Assume that the gravitational-wave signal is an exponentially decaying sinusoid with a frequency f and characteristic damping time scale τ . The wave strain h can then be expressed as

$$h = \frac{1}{2\pi d f} \left(\frac{4G E}{c^3 \tau} \right)^{1/2}, \quad (22)$$

where we have used $\dot{E} \approx E/\tau$ and $\dot{h} \approx 2\pi f h$. Here E is the total energy radiated through the oscillation mode. Measuring the signal through $N_c \approx f\tau$ cycles can boost the signal strength by a factor of $\sqrt{N_c}$. Hence, it is common to define an effective gravitational-wave amplitude by $h_{\text{eff}} \equiv \sqrt{f\tau} h$:

$$h_{\text{eff}} \approx \frac{1}{2\pi d} \left(\frac{4G E}{c^3 f} \right)^{1/2}. \quad (23)$$

Note that h_{eff} depends only on the energy and frequency of the oscillation mode.

Model	Δ (MeV)	f (Hz)	ALIGO	ALIGO	ET	ET
			S/N (Crab)	S/N (Vela)	S/N (Crab)	S/N (Vela)
A	5	351.8	0.3 – 1.0	8.5 – 26.7	4.3 – 13.5	110.3 – 348.8
	10	703.7	0.05 – 0.2	1.4 – 4.4	1.1 – 3.5	28.9 – 91.2
	20	1407.3	0.01 – 0.04	0.3 – 1.0	0.3 – 0.9	7.2 – 22.8
B	5	505.5	0.1 – 0.4	3.1 – 9.9	2.1 – 6.8	55.4 – 175.2
	10	1010.9	0.02 – 0.08	0.6 – 1.9	0.5 – 1.7	14.0 – 44.2
	20	2021.9	0.006 – 0.02	0.1 – 0.5	0.1 – 0.4	3.5 – 11.0
C	5	1253.5	0.02 – 0.05	0.4 – 1.2	0.4 – 1.1	9.1 – 28.7
	10	2506.9	0.004 – 0.01	0.1 – 0.3	0.09 – 0.3	2.3 – 7.1
	20	5013.9	0.0009 – 0.003	0.02 – 0.07	0.02 – 0.07	0.6 – 1.8

TABLE II: Signal-to-noise ratios S/N for the fundamental torsional oscillation modes of the three stellar models listed in Table I. S/N are tabulated for both the Advanced LIGO (ALIGO) and Einstein Telescope (ET). S/N (Crab) corresponds to the value for a Crab glitch. The lower (upper) limit for each S/N data is obtained by assuming that 10% (100%) of the glitch energy is channeled to the mode. Similarly, S/N (Vela) corresponds the value for a Vela glitch.

While the torsional oscillation modes are damped very slowly by gravitational-wave emission, they could nevertheless be damped much faster by internal dissipation. In the Appendix, we provide an order-of-magnitude estimate for the damping time scale due to internal dissipation τ_v and show that $f\tau_v \sim 10^2 - 10^3$ for the oscillation modes studied by us. Assuming $f\tau \gg 1$, the signal-to-noise ratio for the gravitational-wave signal can be estimated by [21]

$$\left(\frac{S}{N}\right) \approx \frac{1}{df} \left[\frac{G}{2\pi^2 c^3} \frac{E}{S_h(f)} \right]^{1/2}, \quad (24)$$

where $S_h(f)$ is the noise power spectral density of the detector. For the Advanced LIGO, $S_h(f)$ is given approximately by (see Table 1 of [54])

$$S_h(f) = S_0 \left[x^{-4.14} - 5x^{-2} + \frac{111(1 - x^2 + 0.5x^4)}{1 + 0.5x^2} \right], \quad (25)$$

where $S_0 = 1.0 \times 10^{-49} \text{ Hz}^{-1}$ and $x = f/215 \text{ Hz}$. On the other hand, for a third-generation detector such as the Einstein Telescope, $S_h(f)$ is given by (see Table 1 of [54])

$$S_h(f) = S_0 \left[x^{-4.1} + 186x^{-0.69} + \frac{233(1 + 31x - 65x^2 + 52x^3 - 42x^4 + 10x^5 + 12x^6)}{1 + 14x - 37x^2 + 19x^3 + 27x^4} \right], \quad (26)$$

where $S_0 = 1.5 \times 10^{-52} \text{ Hz}^{-1}$ and $x = f/200 \text{ Hz}$ in this

case.

For a given mode frequency and distance to the source, the study of the detectability of a gravitational-wave signal now reduces to the problem of finding a reasonable estimate for the energy radiated by the oscillation mode. For the f modes of traditional neutron stars, the energy in the mode must be at least $\sim 10^{-5} M_\odot c^2$ in order for the mode to be marginally detectable by Advanced LIGO [21]. While this amount of energy in the f mode might be possible for wildly pulsating newborn neutron stars formed after supernova explosions, this is not the case for mature compact stars with a crystalline quark core

that we consider in this work. A more relevant energy scale for us is the energy associated with a pulsar glitch. The released energy can be estimated by [41]

$$E_{\text{glitch}} \approx I\Omega\Delta\Omega, \quad (27)$$

where Ω is the angular velocity of the star and $\Delta\Omega$ is the change of Ω in a glitch event. For simplicity, we shall take the moment of inertia $I \sim 10^{45} \text{ g cm}^2$ for the entire star. We shall focus on two well-known pulsars, the Crab and Vela pulsars, in the following analysis. For the Crab (Vela) pulsar, we have $d = 2$ (0.3) kpc, $\Omega =$

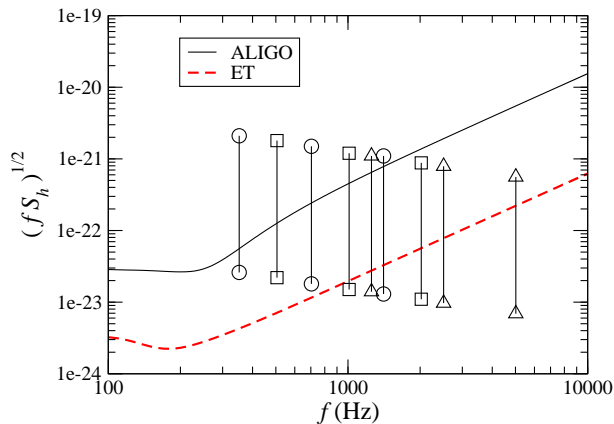


FIG. 9: Effective gravitational-wave amplitudes h_{eff} (vertical lines) for the modes listed in Table II are compared to the dimensionless noise amplitudes $\sqrt{fS_h}$ for both the Advanced LIGO (ALIGO) and Einstein Telescope (ET). For each vertical line, the lower limit is obtained by assuming that 10% of the energy of a Crab glitch is channeled to the mode. The upper limit assumes that 100% of the energy of a Vela glitch is channeled to the mode.

190.4 (70.6) rad s^{-1} , and $\Delta\Omega/\Omega = 10^{-8}$ (10^{-6}). The released energies are then estimated to be $2 \times 10^{-13} M_{\odot} c^2$ and $3 \times 10^{-12} M_{\odot} c^2$ for the Crab and Vela pulsars, respectively. Assuming that a torsional oscillation mode excited in a glitch event carries a similar amount of energy, we can then estimate the signal-to-noise ratio by Eq. (24). In Table II, we summarize the signal-to-noise ratios for the fundamental ($n = 0$) torsional oscillation modes of the three stellar models considered in Sec. IV. We have considered both the Advanced LIGO and Einstein Telescope in the calculations. In the table, S/N (Crab) corresponds to the signal-to-noise ratio for a Crab glitch. Similarly, S/N (Vela) is the value for a Vela glitch. The lower (upper) limit for each S/N data represents the result obtained by assuming that 10% (100%) of the glitch energy is channeled to the oscillation mode.

If we assume that a signal-to-noise ratio must be at least about 10 in order for a gravitational-wave signal to be detectable, Table II shows that the modes of all three stellar models for a Crab glitch are not detectable by Advanced LIGO. However, for a Vela glitch, the mode becomes detectable for models A and B if the gap parameter Δ is at the lower end of the theoretically allowed range near 5 MeV. For stellar model C, which has a small quark core, the modes are not detectable by Advanced LIGO for the entire range of Δ . Comparing to Advanced LIGO, the signal-to-noise ratios typically increase by 1 order of magnitude for the Einstein Telescope as shown in Table II. For this detector, we see that modes for a Crab glitch could also be detectable if the quark core is large and $\Delta \sim 5$ MeV. For a Vela glitch, modes for stellar models A and B should be detectable even for $\Delta \sim 20$ MeV. For model C, however, modes excited in a Vela glitch are detectable only if $\Delta \sim 5$ MeV.

One can also see the general trend of our results from Fig. 9 in which we compare the effective gravitational-wave amplitudes h_{eff} (vertical solid lines) for the modes listed in Table II with the dimensionless noise amplitudes $\sqrt{fS_h}$ for both detectors. For each vertical line in the figure, the lower limit is estimated by assuming that 10% of the energy of a Crab glitch is channeled to the mode. The upper limit assumes that 100% of the energy of a Vela glitch is channeled to the mode. It can be seen that the Einstein Telescope should be able to detect most of the modes in quite general situations. Even more exciting is the possibility that we might already be able to make discoveries with Advanced LIGO.

We end this section by discussing briefly how our results would change for more massive configurations. It should be noted that, for a given EOS model, more massive hybrid stars in general have larger quark cores (see Fig. 4) comparing to those in our canonical $1.4 M_{\odot}$ models. As remarked in Sec. IV B, the frequency of a torsional shear mode is $f \sim v_s/2\pi R_c$. For a given EOS model and gap parameter, the wave speed $v_s = [\mu/(\rho + P)]^{1/2}$ at the surface of the quark core is the same for configurations with different masses, since the transition density from nuclear matter to quark matter is fixed. If we approximate the frequency by evaluating v_s at R_c , the frequency of a torsional oscillation mode for more massive stars, and hence larger R_c , should in general be smaller than that of the canonical model with the same EOS and gap parameter.

As seen in Table II, a smaller mode frequency would in general increase the signal-to-noise ratio, and hence more massive hybrid stars should be more favorable for gravitational-wave detection. For instance, the frequency of the fundamental mode of the $1.63 M_{\odot}$ stellar model shown in Fig. 4 is 328 Hz for $\Delta = 5$ MeV. This frequency is about a factor of 0.65 smaller than the corresponding mode frequency (505.5 Hz) of stellar model B. We note that this agrees quite well with our expectation that the mode frequency should be smaller by a factor of 0.7 according to the scaling relation $f \sim 1/R_c$. As a result of a smaller mode frequency, the upper limit of S/N (Vela) for Advanced LIGO is increased to 32.5 for the $1.63 M_{\odot}$ model, which is about three times higher than that of stellar model B. Finally, as mentioned in Sec. IV A, massive hybrid stars ($M \sim 2 M_{\odot}$) have been constructed from the NJL model [27, 49]. Since the size of the quark core ($R_c \approx 7$ km) and the transition density from nuclear matter to quark matter ($\approx 10^{15} \text{ g cm}^{-3}$) of the resulting stars are close to those of our models (see Fig. 4 of [27]), we expect that massive stars based on the NJL model would also have similar ranges of mode frequency and signal-to-noise ratio as those obtained in our study.

VI. CONCLUSIONS

In this paper, we have studied the torsional oscillations of crystalline color-superconducting hybrid stars in

general relativity. The quark matter in the crystalline core is described by a phenomenological EOS model with parameters to account for nonperturbative QCD corrections. The low-density envelope of the star is composed of pure nuclear matter and the phase transition from quark matter to nuclear matter is implemented by using a Maxwell construction.

We have constructed three canonical $1.4M_\odot$ stellar models with different quark-core sizes and studied their quadrupolar ($l = 2$) torsional oscillation modes in details. First we find that the mode frequency depends sensitively on the gap parameter Δ and the size of the quark core. We have also compared the results obtained by the fully relativistic calculations with those obtained by the Cowling approximation. For stellar models with a large quark core ($R_c/R > 0.5$), the two results can differ by as much as 15% for the fundamental modes. However, the difference drops down to about 1% if the star has a small quark core ($R_c/R \sim 0.1$). On the other hand, quite independent on the quark-core size, the two results in general agree very well for higher harmonics.

Depending on the quark-core size and the value of Δ , the frequency of the fundamental torsional oscillation mode can range from a few hundred hertz to a few kilohertz in our study. This frequency range is quite different from those well-studied oscillation modes of traditional neutron stars, such as the f and p modes, with typical frequencies at a few kilohertz. Their relatively low frequencies also put some of the torsional oscillation modes studied in our models within the best sensitivity region of ground-based gravitational-wave detectors. We have studied the prospect for detecting the gravitational-wave signals emitted from these oscillation modes in a pulsar glitch event by assuming that the energy channeled to the fundamental mode is comparable to the total energy released in the event. For a Vela glitch, we find that the Einstein Telescope should be able to make discovery in quite general situations. Furthermore, the signals from a Vela glitch could be detectable by Advanced LIGO if the quark core is large ($R_c/R \gtrsim 0.5$) and the gap parameter is near the lower limit of the theoretically allowed range at $\Delta \sim 5$ MeV. Our optimistic results thus suggest the interesting possibility that we might already be able to probe the nature of crystalline color-superconducting quark matter with the second-generation gravitational-wave detectors when they come online in the next few years.

Finally, we end this paper with a few remarks. (1) As a first investigation of the torsional oscillations of crystalline color-superconducting hybrid stars, we simplify our study by using a simple phenomenological model to describe the quark matter. In future work, it would be interesting to try more realistic models such as the NJL model of [27, 49], which includes the three-flavor crystalline phase consistently. Nevertheless, we believe that our results would not be changed significantly as long as the internal structure of the star (e.g., the size of the quark core) is similar to those stellar models considered

in this work. Moreover, as we pointed out before, the shear modulus that we employ in this work is based on a Ginzburg-Landau expansion to order Δ^2 , and hence its value only fixes the order of magnitude. Until the calculation can be improved, any attempt to calculate the torsional oscillation modes of hybrid stars should be regarded as yielding an estimate only. (2) The standard explanation of pulsar glitches is based on the pinning and unpinning of superfluid vortices in the inner crust of neutron stars [55–57]. In our analysis of the emitted gravitational-wave signals, we assume that glitches are due to the presence of a crystalline quark core inside the star so that the fundamental torsional oscillation mode can be excited to a large amplitude. Future work is needed to study in detail how pulsar glitches may be explained by the presence of a crystalline quark core and whether it could resolve the problem found in [58, 59], where it is shown that superfluid dynamics confined to the inner crust of a traditional neutron star is in fact not enough to explain the glitch phenomenon. (3) We assume that 10%–100% of the total energy released in a glitch event can be channeled to the oscillation mode. This is certainly an *ad hoc* assumption, but it provides us an order-of-magnitude analysis to quantify whether these signals might be detectable or not. A natural extension of this work is to study how large the amplitude of a torsional oscillation mode can be excited in a core-quake scenario of pulsar glitches [2, 3].

Appendix A: Damping Time Scales

In general, there can be different mechanisms acting simultaneously to damp an oscillation mode. The damping time scale τ is controlled mainly by the most effective dissipative mechanism in the system. As we mentioned at the end of Sec. II C, the torsional oscillations are damped very slowly by current-quadrupole gravitational-wave emissions. The damping time can be estimated by [5]

$$\tau_g \sim 30 \left(\frac{GM_c}{R_c c^2} \right)^{-1} \left(\frac{v_s}{c} \right)^{-5} \omega^{-1}, \quad (\text{A1})$$

where M_c is the mass of the solid core. If we take the typical value $\mu \sim 10$ MeV/fm³ [see Eq. (20)] for the shear modulus and evaluate the wave speed v_s at the surface of the quark core R_c , we would obtain $f\tau_g \sim 10^6$ (with f being the mode frequency) and thus gravitational radiation is not an effective damping mechanism for the torsional oscillations. The fact that $f\tau_g \gg 1$ is the reason why the deep minimum in Fig. 1 has such a narrow width.

The oscillation modes are also damped by internal microphysics processes. Dissipative mechanisms in color-superconducting quark matter have been studied mainly for the CFL phase of quark matter (e.g., [60–64]). At very low temperatures, it is expected that dissipative

processes are dominated by phonon-phonon scattering. In particular, the coefficient for the phonon shear viscosity in the CFL phase is [60]

$$\eta \approx 2.5 \times 10^{27} \left(\frac{\mu_q}{400 \text{ MeV}} \right)^8 \left(\frac{T}{10^9 \text{ K}} \right)^{-5} \text{ g cm}^{-1} \text{ s}^{-1}. \quad (\text{A2})$$

On the other hand, dissipative mechanisms in the crystalline phase of quark matter have not been studied (as far as we are aware). We shall proceed by applying the formalism developed in [65] where it is shown that the viscosity of a solid can be treated formally as that of a fluid. The rate of energy dissipation is given by [65]

$$\frac{dE}{dt} = -2 \int f_{\text{dis}} dV, \quad (\text{A3})$$

where the dissipation function f_{dis} is defined by

$$f_{\text{dis}} = \eta \Sigma^{ij} \Sigma_{ij} + \frac{1}{2} \zeta \Theta^2. \quad (\text{A4})$$

The shear tensor Σ_{ij} is

$$\Sigma_{ij} = \frac{1}{2} (\nabla_i v_j + \nabla_j v_i) - \frac{1}{3} g_{ij} \Theta, \quad (\text{A5})$$

where v_i is the velocity and the expansion $\Theta = \nabla_i v^i$. Note that the coefficients η and ζ in Eq. (A4) corresponds to the shear and bulk viscosities, respectively. Given the rate of energy dissipation (A3), we can estimate the damping time scale of an oscillation mode due to internal viscosities by $\tau_v = 2E / |dE/dt|$, where the energy of the mode is $E = \int \rho v^2 dV / 2$ (see, e.g., [64]). Since the amplitude of the fundamental torsional oscillation mode reaches a maximum at the surface of the quark core (see Fig. 6), we shall approximate E and dE/dt by evaluating their integrands at $r = R_c$. Restricting to the torsional

oscillations, where the velocity field is divergence-free, we obtain the following estimate for the damping time scale:

$$\tau_v \sim \frac{\rho(R_c) R_c^2}{\eta}, \quad (\text{A6})$$

where $\rho(R_c)$ is the density at the surface of the solid core and we have also neglected numerical factors of order unity. The value of the coefficient η has not been computed for the crystalline quark matter. As a rough estimate, we take the typical value $\eta \approx 10^{27} \text{ g cm}^{-1} \text{ s}^{-1}$ as suggested in Eq. (A2) for the CFL phase at $T = 10^9 \text{ K}$. Using the typical values $\rho(R_c) \approx 10^{15} \text{ g cm}^{-3}$ and $R_c \approx 5 \text{ km}$ for our canonical models, we obtain the damping time scale due to internal dissipation $\tau_v \sim 0.3 \text{ s}$. Comparing to gravitational-wave damping, our analysis suggests that the torsional oscillation modes would be damped much faster by internal dissipation. However, for the range of mode frequency we studied (see Table II), we obtain $f\tau_v \sim 10^2 - 10^3$ and hence $f\tau \gg 1$ is still a reasonable assumption.

Our analysis is a crude approximation based on the assumption that phonon-phonon scattering in the crystalline phase would not differ significantly from that in the CFL phase. More detailed work in this direction is needed to improve our estimation. In fact, as pointed out in [60], the hydrodynamic treatment of the phonons used in the derivation of Eq. (A2) is not valid anymore in the low-temperature regime, where the mean-free path of phonons would be much larger than the stellar radius. The CFL quark matter would then become a perfect superfluid. If we use the effective shear viscosity suggested in [64], $\eta_{\text{eff}} \approx 5 \times 10^{17} (T/10^9 \text{ K})^4 \text{ g cm}^{-1} \text{ s}^{-1}$, the value of which is obtained by requiring that the mean-free path of phonons is limited by the stellar radius, then the damping time scale at the same temperature 10^9 K would be increased by a factor of 10^9 .

-
- [1] P. Haensel, A. Y. Potekhin, and D. G. Yakovlev, *Neutron Stars 1: Equation of State and Structure* (Springer, New York, 2007).
- [2] D. Pines, J. Shaham, and M. Ruderman, *Nat. Phys. Sci.* **237**, 83 (1972).
- [3] G. Baym, D. Q. Lamb, and F. K. Lamb, *Astrophys. J.* **208**, 829 (1976).
- [4] This is an unpublished remark made by Dyson as quoted in [5].
- [5] B. L. Schumaker and K. S. Thorne, *Mon. Not. R. Astron. Soc.* **203**, 457 (1983).
- [6] D. D. Ivanenko and D. F. Kurdgelaidze, *Astrophysics* **1**, 251 (1965).
- [7] N. Itoh, *Prog. Theor. Phys.* **44**, 291 (1970).
- [8] G. Baym and S. A. Chin, *Phys. Lett. B* **62**, 241 (1976).
- [9] M. Alford, K. Rajagopal, and F. Wilczek, *Phys. Lett. B* **422**, 247 (1998).
- [10] R. Rapp, T. Schäfer, E. V. Shuryak, and M. Velkovsky, *Phys. Rev. Lett.* **81**, 53 (1998).
- [11] M. Alford, K. Rajagopal, and F. Wilczek, *Nucl. Phys.* **B537**, 443 (1999).
- [12] M. Alford and S. Reddy, *Phys. Rev. D* **67**, 074024 (2003).
- [13] M. G. Alford, A. Schmitt, K. Rajagopal, and T. Schäfer, *Rev. Mod. Phys.* **80**, 1455 (2008).
- [14] R. Anglani, R. Casalbuoni, M. Ciminale, R. Gatto, N. Ippolito, M. Mannarelli, and M. Ruggieri, arXiv:1302.4264.
- [15] M. Alford, J. A. Bowers, and K. Rajagopal, *Phys. Rev. D* **63**, 074016 (2001).
- [16] R. Casalbuoni, R. Gatto, N. Ippolito, G. Nardulli, and M. Ruggieri, *Phys. Lett. B* **627**, 89 (2005); *Phys. Lett. B* **634**, 565(E) (2006).
- [17] M. Mannarelli, K. Rajagopal, and R. Sharma, *Phys. Rev. D* **73**, 114012 (2006).
- [18] K. Rajagopal and R. Sharma, *Phys. Rev. D* **74**, 094019 (2006).
- [19] R. Casalbuoni, M. Ciminale, R. Gatto, G. Nardulli, and M. Ruggieri, *Phys. Lett. B* **642**, 350 (2006).
- [20] N. Andersson and K. D. Kokkotas, *Phys. Rev. Lett.* **77**,

- 4134 (1996).
- [21] K. D. Kokkotas, T. A. Apostolatos, and N. Andersson, *Mon. Not. R. Astron. Soc.* **320**, 307 (2001).
- [22] O. Benhar, V. Ferrari, and L. Gualtieri, *Phys. Rev. D* **70**, 124015 (2004).
- [23] L. K. Tsui and P. T. Leung, *Phys. Rev. Lett.* **95**, 151101 (2005).
- [24] H. K. Lau, P. T. Leung, and L. M. Lin, *Astrophys. J.* **714**, 1234 (2010).
- [25] L.-M. Lin, *Phys. Rev. D* **76**, 081502(R) (2007).
- [26] B. Haskell, N. Andersson, D. I. Jones, and L. Samuelsson, *Phys. Rev. Lett.* **99**, 231101 (2007).
- [27] B. Knippel and A. Sedrakian, *Phys. Rev. D* **79**, 083007 (2009).
- [28] K. D. Kokkotas and B. G. Schmidt, *Living Rev. Relativity* **2**, 2 (1999).
- [29] M. Karlovini and L. Samuelsson, *Classical Quantum Gravity* **24**, 3171 (2007).
- [30] G. L. Israel, T. Belloni, L. Stella, Y. Rephaeli, D. E. Gruber, P. Casella, S. Dall’Osso, N. Rea, M. Persic, and R. E. Rothschild, *Astrophys. J.* **628**, L53 (2005).
- [31] A. L. Watt and T. E. Strohmayer, *Adv. Space Res.* **40**, 1446 (2007).
- [32] L. Samuelsson and N. Andersson, *Mon. Not. R. Astron. Soc.* **374**, 256 (2007).
- [33] H. Sotani, K. D. Kokkotas, and N. Stergioulas, *Mon. Not. R. Astron. Soc.* **375**, 261 (2007).
- [34] M. Vavoulidis, A. Stavridis, K. D. Kokkotas, and H. Beyer, *Mon. Not. R. Astron. Soc.* **377**, 1553 (2007).
- [35] H. Sotani, K. D. Kokkotas, and N. Stergioulas, *Mon. Not. R. Astron. Soc.* **385**, L5 (2008).
- [36] A. Colaiuda and K. D. Kokkotas, *Mon. Not. R. Astron. Soc.* **414**, 3014 (2011).
- [37] H. Sotani, K. Nakazato, K. Iida, and K. Oyamatsu, *Phys. Rev. Lett.* **108**, 201101 (2012).
- [38] M. Gabler, P. Cerdá-Durán, N. Stergioulas, J. A. Font, and E. Müller, *Mon. Not. R. Astron. Soc.* **421**, 2054 (2012).
- [39] K. S. Thorne and A. Campolattaro, *Astrophys. J.* **149**, 591 (1967).
- [40] G. L. Comer, D. Langlois, and L. M. Lin, *Phys. Rev. D* **60**, 104025 (1999).
- [41] N. Andersson, G. L. Comer, and D. Langlois, *Phys. Rev. D* **66**, 104002 (2002).
- [42] L.-M. Lin, N. Andersson, and G. L. Comer, *Phys. Rev. D* **78**, 083008 (2008).
- [43] M. Buballa, *Phys. Rep.* **407**, 205 (2005).
- [44] M. Alford, M. Braby, M. Paris, and S. Reddy, *Astrophys. J.* **629**, 969 (2005).
- [45] A. Akmal, V. R. Pandharipande, and D. G. Ravenhall, *Phys. Rev. C* **58**, 1804 (1998).
- [46] F. Douchin and P. Haensel, *Phys. Lett. B* **485**, 107 (2000).
- [47] G. Baym, C. Pethick, and P. Sutherland, *Astrophys. J.* **170**, 299 (1971).
- [48] P. Haensel and B. Pichon, *Astron. Astrophys.* **283**, 313 (1994).
- [49] N. D. Ippolito, M. Ruggieri, D. H. Rischke, A. Sedrakian, and F. Weber, *Phys. Rev. D* **77**, 023004 (2008).
- [50] M. Mannarelli, K. Rajagopal, and R. Sharma, *Phys. Rev. D* **76**, 074026 (2007).
- [51] N. D. Ippolito, G. Nardulli, and M. Ruggieri, *J. High Energy Phys.* **04**, (2007) 036.
- [52] B. J. Owen, *Phys. Rev. Lett.* **95**, 211101 (2005).
- [53] N. K. Johnson-McDaniel and B. J. Owen, *Phys. Rev. D* **88**, 044004 (2013).
- [54] B. S. Sathyaprakash and B. F. Schutz, *Living Rev. Relativity* **12**, 2 (2009).
- [55] P. W. Anderson and N. Itoh, *Nature (London)* **256**, 25 (1975).
- [56] M. A. Alpar, P. W. Anderson, D. Pines, and J. Shaham, *Astrophys. J.* **276**, 325 (1984).
- [57] M. A. Alpar, P. W. Anderson, D. Pines, and J. Shaham, *Astrophys. J.* **278**, 791 (1984).
- [58] N. Andersson, K. Glampedakis, W. C. G. Ho, and C. M. Espinoza, *Phys. Rev. Lett.* **109**, 241103 (2012).
- [59] N. Chamel, *Phys. Rev. Lett.* **110**, 011101 (2013).
- [60] C. Manuel, A. Dobado, and F. J. Llanes-Estrada, *J. High Energy Phys.* **09**, (2005) 076.
- [61] M. G. Alford, M. Braby, S. Reddy, and T. Schäfer, *Phys. Rev. C* **75**, 055209 (2007).
- [62] M. Mannarelli, C. Manuel, B. A. Sa’d, *Phys. Rev. Lett.* **101**, 241101 (2008).
- [63] M. Mannarelli and C. Manuel, *Phys. Rev. D* **81**, 043002 (2010).
- [64] N. Andersson, B. Haskell, and G. L. Comer, *Phys. Rev. D* **82**, 023007 (2010).
- [65] L. D. Landau and E. M. Lifshitz, *Theory of Elasticity* (Pergamon Press, New York, 1986).